

Experimental and Numerical Investigation on Shell-side Performance of Multilayer Spiral-Wound Heat Exchangers

Xing Lu, Xueping Du, Sen Zhang, Min Zeng, Qiuwang Wang*

Key Laboratory of Thermo-Fluid Science and Engineering, Ministry of Education, Xi'an Jiaotong University, Xi'an 710049, China
wangqw@mail.xjtu.edu.cn

Considering extensive applications of multilayer spiral-wound heat exchangers (SWHEs) in industry but insufficient focus on shell-side fluid in SWHEs, an experimental investigation on flow and heat transfer performances in the shell-side of a self-manufacturing SWHE with 3 layers of coil inside the cylinder shell is carried out. Numerical simulation using constant heat flux boundary condition is also performed. The flow and heat transfer characteristics on the shell-side of the multilayer SWHE are obtained, and then relevant empirical correlations of $Nu = 0.0193 \cdot Re^{0.816}$ and $f_s = 0.401 / Re^{0.197}$ are achieved. The results from CFD method gives visualization of flow and heat field of shell-side in the 3-layer SWHE and provides a reasonable estimation of flow and heat transfer performance.

1. Introduction

The spiral-wound heat exchangers are widely used in air separation plants, chemical process and nuclear industry due to their highly compact structure, large heat transfer area per unit volume, high pressure endurance, and multi-stream heat transfer etc. Using helical coils in heat exchangers is an effect way for heat transfer enhancement. However, much investigation has been carried out on heat transfer coefficients inside coiled pipes, and little work has been reported on the shell-side heat transfer coefficient. Ever since Eustice J (1911) first observed a secondary flow of water flow in the curved pipe in his experiment, much investigation on helix pipes has been performed and the mechanism of secondary flow is clear. However, in engineering fields, the manufacturing of multilayer SWHEs remains some problems on the characteristics and mechanisms of the shell-side flow and heat transfer, and needs more information for further optimization of SWHEs' performance in heat transfer. Ghorbani et al. (2010) implemented an experimental study on mixed convective heat transfer under various Reynolds number, curvature ratio and pitch, and made a discussion on the influence of difference geometrical parameters on heat transfer performance. Different definitions of characteristic length were analyzed and the shell-side equivalent diameter was taken as the most reasonable one. Moawed et al. (2011) investigated the influence of various curvature and torsion rate on outer-side heat transfer coefficient. The experiment model was a vertical heat exchanger whose coil was wound by hollow pipe inserted with electric heating wire. Picón-Núñez et al. (2012) developed the graphical design method originally applied for shell and tube heat exchangers and extended to the case of spiral heat exchangers which have similar and simpler structure than the multilayer SWHEs. Neeraas et al. (2004) published some experimental results of pressure drop and heat transfer in a 3-layer spiral-wound LNG heat exchangers unit. But only the performance under low-temperature working condition was published.

The present work aims to study the shell-side flow characteristic and heat transfer performance in multilayer SWHEs. A self-designed and self-manufactured SWHE model is tested in the experimental study, and the selection of geometrical parameter is within the industrial application ranges. The numerical model has the same specification as the experimental one.

2. Characteristic of spiral-wound heat exchangers

2.1 Basic construction

Figure 1 gives a simplified physical model of a multilayer SWHE. In the space between the outer shell and the center cylinder, coils are wound reversely between adjacent layers and are fixed by space bars in each layer. The pipe has an outer diameter D_t . The coil has a pitch pl , representing the longitudinal distance between two adjacent turns, while the axial distance is pr . The angle that projection of one turn of the coil makes with a plane perpendicular to the axis, is named as the helix angle, α . The space bar thickness is B . The coil has a diameter of D_c (measured between the centres of adjacent pipes). The outer diameter of centre cylinder and the inner diameter of shell are $D_{s,i}$ and $D_{s,o}$, respectively. An effective height for heat transfer, H , is defined when the height of a spiral-wound heat exchanger needed.

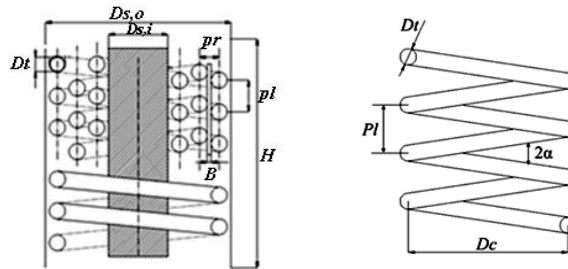


Figure 1: Basic geometries of a multilayer SWHE

2.2 Multilayer spiral-wound heat exchanger manufacturing

A set of multilayer spiral-wound heat exchanger is designed and manufactured. The effective height of the heat exchanger H is 300 mm, and the straightening length between the entrance and outlet is 100 mm, respectively. The present spiral-wound heat exchanger has 4 pipes in the innermost layer (the first layer, $N_c=4$), 5 pipes in the middle layer (the second layer, $N_c=5$) and 6 ones in the outermost layer (the third layer, $N_c=6$). The numbers of turns in each layer are 3.6, 3.1 and 2.8, respectively. In engineering applications, the space bar thickness ranges from 1 mm to 4 mm, the helix angle 5° to 15° , the outer diameter of pipe 8 mm to 19 mm, and the pitch of coil 8 mm to 20 mm. The selection of geometrical parameters is within the industrial application ranges. The geometrical parameters of the experimental model are shown in Table 1.

Table 1: Multilayer Spiral-wound Heat exchanger specifications (Unit: mm)

No.	$D_{s,o}$	$D_{s,i}$	D_t	D_c	pl	Turns	Angle	N_c	Helix direction
1	243	159	10	175	20.85	3.6	8.53	4	Left-hand
2	243	159	10	201	19.16	3.1	8.53	5	Right-hand
3	243	159	10	227	18.03	2.8	8.53	6	Left-hand

The coils are bent by using copper electric heating pipes and are enclosed by a cylinder shell to provide a shell-side fluid passage. Via applying fixed electric power for the coils, the third kind of boundary condition (constant heat flux) can be realized. In the present work, an electric power of 950 W is provided and the total area of the outer surface of the coils is 0.95 m^2 , which makes a constant heat flux of $1,000 \text{ W/m}^2$ on the outer walls of coils.

3. Experiment apparatus

3.1 Experimental setup

The experiment study is carried on in a wind tunnel laboratory. The test section of SWHE is connected to an open system which is consisted of entrance, straightening section of inlet and prolongation section of outlet, blower and measure instruments, providing necessary flows through the shell of the system and the required measure facilities. Figure 2 illustrates the wind tunnel testing system.

Nine copper-constantan thermocouples are evenly set on the inlet and outlet of the test system, respectively, to measure the inlet and outlet fluid temperature. There are five sets of multi-point copper-constantan thermocouples set on five cross-sections of spiral-wound heat exchanger along the axial direction, respectively, and each set contains six thermocouples. Figure 3 illustrates the relevant locations of the five cross-sections.

A glass rotameter is employed to measure volume flow rates of the air. Copper-constantan compensating conductors are connected to the data acquisition board and temperature-constant furnace is used to

achieve cold end compensation. Microbarometer with a minimum scale of 2 Pa at small flow rates and U-tube water column manometer at big flow rates are used to obtain pressure data. The electric power applied for the pipes is measured by a wattmeter. A voltage regulator, whose range is 0 V~220 V, is used for regulating the value of electric power. An ammeter is connected in the electric circuit to check whether the current is overload or not for the safety of the experiment system.

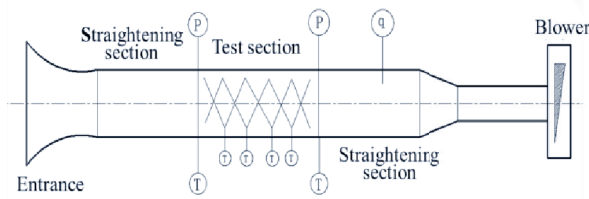


Figure 2: Experimental setup

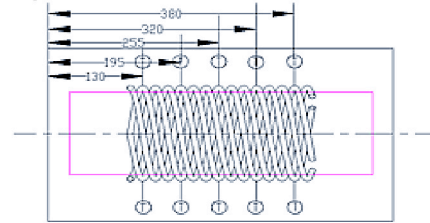


Figure 3: Relevant locations of thermocouples in 5 cross-sections

3.2 Experimental procedure

Each flange in the system is sealed by rubber gaskets. Heat insulation cotton with a thickness of 2 cm is wrapped around the shell of test section to minimise heat loss. Much attention is paid to the heat balance to ensure the steady state of heat exchange before writing down the data during implementing the experiment. The energy gain of the air and the electric power are used to calculate the heat balance error, which is within 5 % in each trials of test. During the experiment process, the heat transfer rates of the pipes keep constant (1,000 W/m²) by applying a steady electric power, and the volume flow rate of the air varies from 60 m³/h to 160 m³/h. More than 3 h is needed to attain a steady state at the beginning of the experiment and steady states of the following trials are achieved within 2~3 h.

3.3 Data reduction

The heat flux on the surface of electric pipes, Φ_t , is obtained directly from the wattmeter. The heat absorbed by the air, Φ_s , can be calculated by the inlet and outlet temperature and mass flow rate. It is assumed that the air temperature changes linearly along the axial direction in the test model. The local air temperature, T_i , is evaluated by linear interpolation methods. Then the local heat transfer coefficient and local Nusselt number can be acquired.

$$h = \frac{(\Phi_t + \Phi_s)}{2} \cdot \frac{1}{A \cdot (T_w - T_i)} \quad (1)$$

$$Nu = \frac{h \cdot D_t}{\lambda} \quad (2)$$

The minimum flow area of shell-side in multilayer SWHE, $A_{s,min}$, is calculated by Naphon P et al. (2006),

$$A_{s,min} = \pi \cdot \left(\frac{D_{s,i} + D_{s,o}}{2} \right) \cdot N_c \cdot B \quad (3)$$

Then the maximum fluid velocity, u_m , could be calculated. Reynolds number and friction coefficient are defined as,

$$Re = \frac{\rho \cdot u_m \cdot D_t}{\mu} \quad (4)$$

$$f_s = \frac{2 \Delta p \cdot D_t}{\rho \cdot u_m^2 \cdot H} \quad (5)$$

The maximum experimental uncertainties of Nusselt number and friction coefficient are 5.7 % and 5.4 %, respectively.

4. Numerical simulation

CFD estimation is employed to analyze the flow and heat transfer performances in the multilayer SWHE. The geometry model used for numerical simulation is the same as the experimental model and the inlet and outlet are prolonged more than 10 times of the characterized length of the heat exchanger to avoid the entrance effect and reversed flow, respectively.

4.1 Grid and boundary conditions

The geometrical model is created by ProE software. The mesh is generated using ICEM of the ANSYS 14.0 package. In the numerical model, the unstructured grid is generated for the shell-side fluid area due

to its highly irregular structure. Figure 4 shows the grid of shell-side fluid area for the numerical analysis domain and detailed image of meshes on the coil.

The outer walls of the pipes are defined as wall boundary condition with constant heat flux of $1,000 \text{ W/m}^2$, which is the same as the electric power in the experiment. For momentum equation, they are taken as no-slip walls and the inner wall of the shell and the outer wall of the centre cylinder are treated as no-slip adiabatic walls. The fluid inlet area is defined as velocity inlet boundary condition and fluid outlet area is set as pressure outlet with zero back flow pressure.

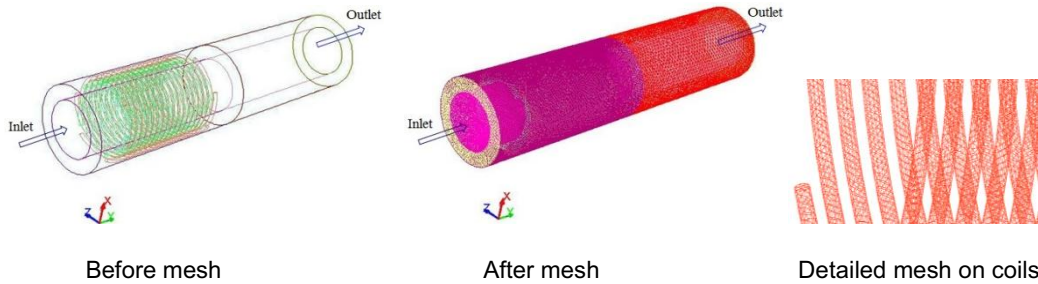


Figure 4: Grids of shell-side fluid domain

4.2 CFD modelling

The fluid flow performance of the shell-side and the heat exchange between the shell-side fluid and the wall of coil with a constant heat flux are calculated by FLUENT 14.0. Air inlet flow rate and temperature are set the same value as the experiment value. The RNG $k-\epsilon$ turbulence model with standard wall functions is used for CFD simulation. Grid independence of the domain is established. The total grids of the shell-side are changed from 1,306,308 to 2,432,180. The same CFD calculation conditions are used in these three set of meshes and the average Nusselt number of the shell-side is checked for the grid independence validation. The results show that the error between the mesh with 1,888,150 grids and the one with 2,432,180 grids is lower than 2 %. So the optimum mesh with 1,888,150 grids is employed for further analysis. It has 328,845 nodes, 3,240,973 faces and 1,538,809 cells.

5. Results and discussion

Figure 5 (a) indicates that the local heat transfer coefficient in different cross-section increases when Re increases. It shows that the entrance section has higher heat transfer coefficient. Since the change of Prandtl number can be ignored in the present study, the variation of local Nusselt number is similar to that of local heat transfer coefficient. As shown in Figure 5 (b), it can be noticed that the local heat transfer coefficients decrease along the cross section of flow direction. Also, the inlet location has a much higher heat transfer coefficient than that of the other four locations. The reason may be that the electric insulation tapes wrapped on the ends of pipes to avoid electric leakage will cause that the measurement temperature is lower than the reality. Another main reason is that the air blow from the flared inlet encounters a reducing duct, resulting in a sudden increase of velocity and then the heat transfer is more enhanced in the inlet position.

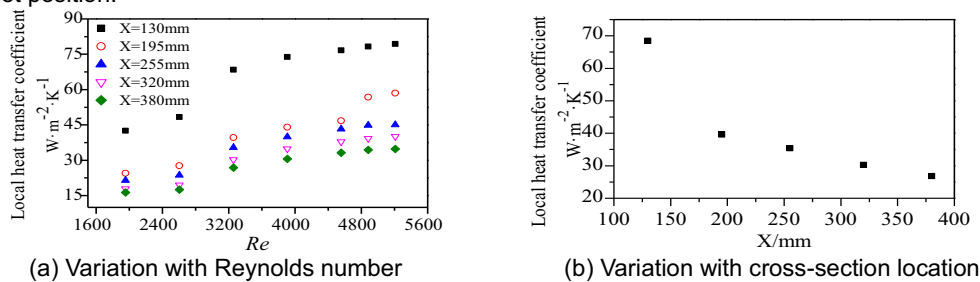


Figure 5: Local heat transfer coefficient

The average Nusselt number of the 3-layer SWHE is compared with that of the monolayer SWHE (Xin et al., 1997). Fig 6 shows that the heat transfer performance of the multilayer SWHE is better than that of the monolayer one. Figure 7 depicts the change of pressure drop and friction coefficient of the shell-side. The present work uses a fitting method under logarithmic coordinate to obtain the experimental correlations:

$$Nu = 0.0193 \cdot Re^{0.816} \quad (6)$$

$$f_s = 0.401 / Re^{0.197} \tag{7}$$

where the range of Re is $1,500 < Re < 5,500$.

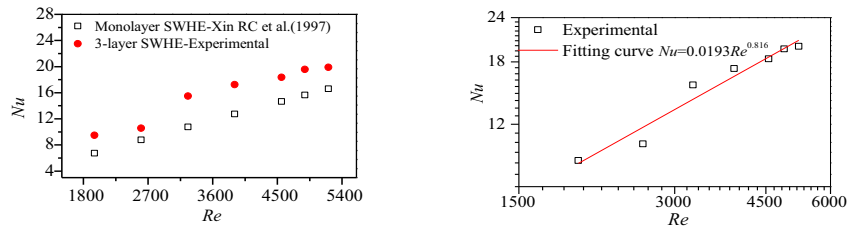


Figure 6: Nusselt number vs. Reynolds number

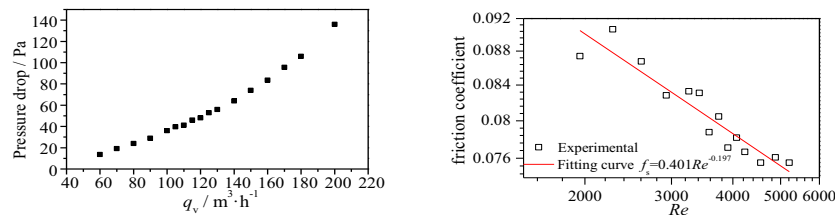


Figure 7: Pressure drops and friction coefficients

CFD method provides with a clear display of the fluid flow and temperature fields in the calculation domain. Fig 8 illustrates the pathlines of the near wall area of the coils. The pathlines in the entrance part is a little irregular and become smooth after a short flow distance. Figs 9 and 10 show the temperature and pressure fields on the wall of pipes. The temperature decreases from inlet to outlet. It can be also seen that temperature difference on the same cross section is significant. This could explain that why the previous experiment measures have big temperature difference on the same cross-section of the wall for heat transfer.



Figure 8: Pathlines

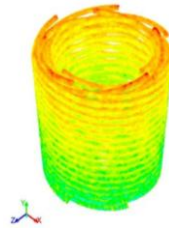


Figure 9: Temperature contours

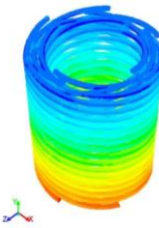


Figure 10: Pressure contours

Air temperature in the shell is hard to be measured directly in the experiment. So during the experimental data reduction, it is assumed that the fluid temperature changes linearly along the axial direction. But the feasibility of this assumption needs a reasonable explanation. The advantage of CFD estimation is that the average fluid temperature in each cross section can be obtained from the calculation results. Figure 11 reveals the variation of the average fluid temperature along axial direction. Under each flow rate, the variation of the average fluid temperature is linear, which proves that the linear assumption is acceptable.

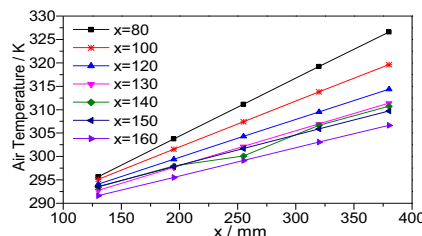


Figure 11: Air temperature along axial passage of shell-side

Figure 12 (a) compares the temperature differences between the inlet and the outlet of experiment with those of simulation. It can be found that the deviations of the temperature differences from the experiment

between the ones from the simulation are lower than 6.4 %. As shown in Figure 12 (b), the errors of average heat transfer coefficients are below 13.4 % when Re is within the range of 3,000~5,500, while the deviation between the experimental data and simulation result is much big when $Re=2,604$. Different way of wall temperature averaging may cause big errors, for the wall temperature of experiment is only from 5 measurement points but that of CFD is from the whole nodes meshed on the wall of the coil. Also, since the critical Reynolds number for shell-side fluid in multilayer SWHEs has not been clarified, the turbulence model employed in the numerical model may be not applicable under relatively low Reynolds flow patterns.

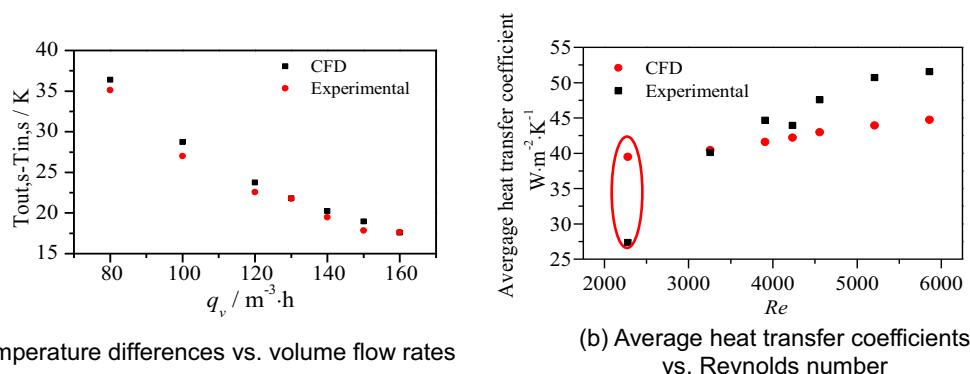


Figure 12: Temperature differences and average heat transfer coefficients of simulation vs. experiment

6. Conclusions

Due to insufficient focus on shell-side fluid in multilayer spiral-wound heat exchangers, an experimental investigation on flow and heat transfer performances in shell-side of a self-designed and self-manufacturing SWHE with 3-layer coil inside the cylinder shell is performed. In terms of data reduction, the CFD result proves that the linear assumption of the air temperature changing trend along the axial direction is reasonable. CFD also assist to give visualized images of flow and heat fields. The experiment data shows that the heat transfer performance in multilayer SWHEs is better than that in monolayer ones. The experiment provides some initial data for flow and heat transfer on shell-side fluid under constant heat flux boundary condition. Empirical correlations for Nusselt number and friction coefficient are obtained.

Acknowledgements

This work is supported by the International Cooperation and Exchanges Project of NSFC of China (Grant No. 51120165002), the National Natural Science Foundation of China (Grant No. 51276139).

References

- Eustice J., 1911. Experiment of streamline motion in curved pipes, Proceedings of Royal Society of London: Series A, 85, 119-131, DOI: 10.1098/rspa.1911.0026.
- Ghorbani N., Taherian H., Gorji M., Mirgolbabaee H., 2010. Experimental study of mixed convection heat transfer in vertical helically coiled tube heat exchangers, Experimental Thermal and Fluid Science, 34, 900-905, DOI: 10.1016/j.expthermflusci.2010.02.004.
- Moawed M., 2011. Experimental study of forced convection from helical coiled tubes with different parameters, Energy Conversion and Management, 52, 1150-1156, DOI: 10.1016/j.enconman.2010.09.009.
- Naphon P., Wongwises S., 2006. A review of flow and heat transfer characteristics in curved tubes, Renewable and Sustainable Energy Reviews, 10, 463-490, DOI: 10.1016/j.rser.2004.09.014.
- Neeraas B.O., Fredheim A.O., Aunan B., 2004. Experimental shell-side heat transfer and pressure drop in gas flow for spiral-wound LNG heat exchanger, International Journal of Heat and Mass Transfer, 47, 353-361, DOI: 10.1016/S0017-9310(03)00400-9.
- Picón-Núñez M., Polley G.T., Riesco-Ávila J.M., 2012. Design space for the sizing and selection of heat exchangers of the compact type, Chemical Engineering Transactions, 29, 217-222, DOI: 10.3303/CET1229037.
- Xin R.C., Ebdian M.A., 1997. The effects of Prandtl numbers on local and average convective heat transfer characteristics in helical pipes, Journal of Heat Transfer, 119, 463-467, DOI: 10.1115/1.2824120.